# USE OF MAGNETIC COMPRESSION TO SUPPORT TURBINE ENGINE ROTORS

**Squadron Leader Chris J Pomfret, Royal Air Force**
**Wright Laboratory**
**Wright-Patterson AFB OH 45433-7251**



## ABSTRACT

Ever since the advent of gas turbine engines, their rotating disks have had to be designed with sufficient size and weight to withstand the centrifugal forces generated when the engine is operating. Unfortunately, this requirement has always been a life and performance limiting feature of gas turbine engines and, as manufacturers strive to meet operator demands for more performance without increasing weight, the need for innovative technology has become more important. This has prompted engineers[1] to consider a fundamental and radical breakaway from the traditional design of turbine and compressor disks which have been in use since the first jet engine was flown 50 years ago. Magnetic compression aims to counteract, by direct opposition rather than restraint, the centrifugal forces generated within the engine. A magnetic coupling is created between a rotating disk and a stationary superconducting coil to create a massive inwardly-directed magnetic force. With the centrifugal forces opposed by an equal and opposite magnetic force, the large heavy disks could be dispensed with and replaced with a torque tube to hold the blades. The proof of this concept has been demonstrated and the thermal management of such a system studied in detail; this aspect, especially in the hot end of a gas turbine engine, remains a stiff but not impossible challenge. The potential payoffs in both military and commercial aviation and in the power generation industry are sufficient to warrant further serious studies for its application and optimization.

## MECHANICS OF MAGNETIC COMPRESSED ROTORS (MCR)

Magnetic forces arise when electrical current flow is orthogonal to a magnetic field. Figure 1 shows the

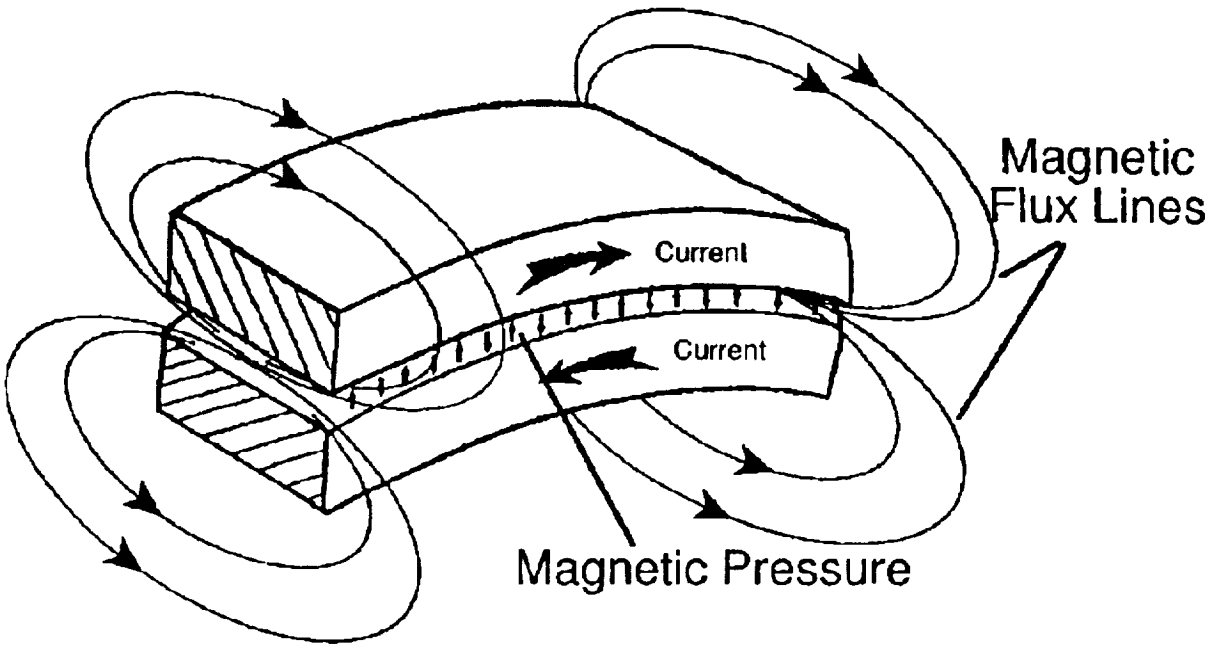


Figure 1: Opposing Currents Generate Repulsive Loads

[1]Small Business Innovative Research program for Wright Laboratory, Wright-Patterson AFB OH by IAP Research Inc., Dayton OH. Technical Reports WRDC-TR-90-2088 "Magnetically Compressed Ring" and WL-TR-93-2014 "Magnetically Compressed Ring Thermal Management System Demonstration" refer.

principle for two conductors carrying oppositely directed currents. Each conductor generates its own magnetic flux and the interaction of the magnetic flux with the current in the opposite conductor creates a magnetic body force within each. As long as opposing currents flow in each conductor, the magnetic body force or "magnetic pressure" will repel the conductors from each other. If the conductors are rings then the inner ring will be in compression and the outer ring in tension. The concept of MCR has been founded on this principle.

Expanding the concept to gas turbine engines is depicted in Figure 2. The inner conducting ring, referred to as the armature conductor, rotates with the blades and supports the centrifugal loads. Magnetic pressure between the armature conductor and the stationary outer conductor (excitation conductor) transmits the centrifugal load to the outer conductor. A structural hoop wrapped around the outside of the excitation conductor ultimately supports the centrifugal loads.

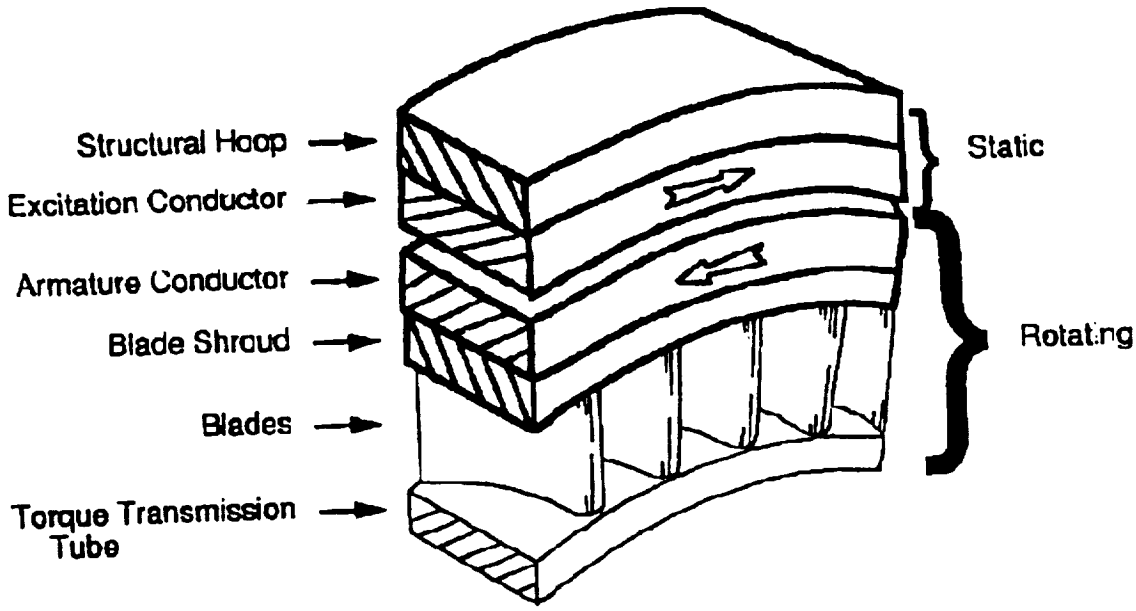


Figure 2: Centrifugal Loads are Transferred to a Static Structural Hoop

## THE PERCEIVED BENEFITS OF MCR

There are clearly many challenges associated with a real-life, commercial, application of this concept and these will be addressed later. The many potential benefits are considered first.

### Advanced Materials

We envision an increasing utilization of lighter weight materials such as ceramics and composites in future gas turbine engines. These advanced materials enjoy compressive rather than tensile forces. Using MCR, compressor and turbine blades would be in compression during operation.

### Weight Savings

Although a detailed weight saving benefit analysis has not been carried out, there is an obvious potential for significant weight reductions. A turbine disk typically weighs 150 lbs; this would be dispensed with and replaced by a torque tube of much lighter weight. While the weight of the superconducting assembly would need to be added in, removal of obsolete bearing and lubrication equipment would provide further weight saving advantages. Based on rough approximations using the F110 engine, Figure 3 compares the weights of disks by

stage and the estimated weights of the MCR components which would be introduced. Savings in the region of 20% could be achieved for a HP Turbine first stage application (stage 13) whereas weight would be added if applied to a fan (stage 1). This assessment is very approximate and ongoing enhancements to superconductor technology would further increase the perceived benefits. The "MCR Dry" bar shows the complete system weight whereas the "MCR Rotating" bar is for the inner assembly only (torque tube, blades, insulation, armature etc.).

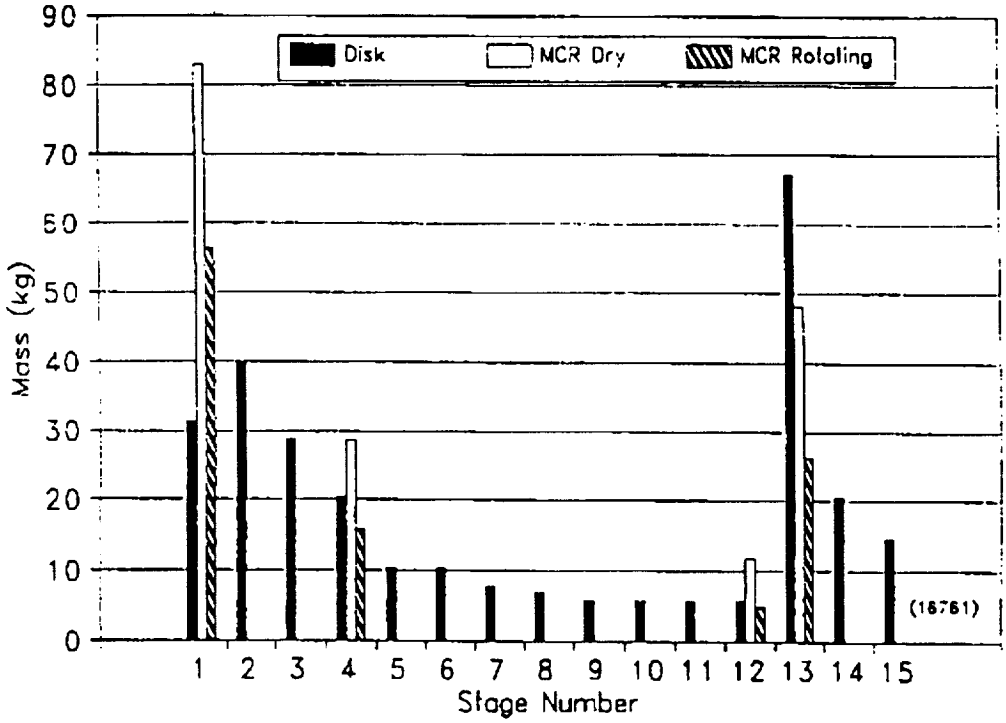


Figure 3: Comparison of Masses of MCR Components with Current F110 Disks

Performance Increases

Performance of gas turbine engines has always been limited by rotational speed constraints of compressor and turbine disks and the associated loads on bearings. Disposing of disks and bearings will permit increased rotational speeds and therefore increased performance. The perceived performance increases coupled with the weight reductions outlined above would make a significant impact on the Integrated High Performance Turbine Engine Technology (IHPTET) Initiative which aims to double the propulsive capability (thrust/weight ratio) of gas turbine engines in the next 10 years.

System Simplicity

Support features of a conventional gas turbine engine could be simplified or removed. There would no longer be a need for a bearing and lubrication system. The cost of design, purchase and upkeep of these features would thus be eliminated. Similarly, the significant design, manufacture and maintenance costs of disks would be zeroed. Currently, a great deal of cost and effort goes into life prediction, life measurement and inspection of disks so that their fatigue life is not exceeded. With the advent of two-level maintenance in the Air Force, equipment simplification and reduced maintenance activity are becoming more important and attractive. We believe that the simplifications cited above will be greater than the extra costs and upkeep created by the introduction of the superconducting equipment.

Life Availability

Currently, hot-end components are the major life limiting features of gas turbine engines. With MCR, increases in safe and useful life could be expected from the rotating components especially if metallic blades are replaced by advanced materials. The effects on life cycle costs would be significant; affordability would also be enhanced.

More Electric Aircraft (MEA) Initiative

Running in parallel with IHPTET is another initiative which, in its aim to increase aircraft reliability, supportability and maintainability, proposes fundamental changes to power subsystems. One such proposal is to remove the conventional hydraulic systems from aircraft and replace them with more reliance on electrical control and actuation. We have considered the interaction of MCR with the More Electric Aircraft (MEA) Initiative and found the two concepts to be, in theory, compatible. MEA would benefit from MCR by using the superconducting rings as an energy storage subsystem to prevent surges, ripples, and interruptions from the aircraft power supply. High temperature superconductor technology and cooling technology would be similar for the development of both concepts. Finally, the power requirements for spooling-up an MCR equipped engine (superconductor charge) would, at 300 kW, not exceed the perceived capacity of ground power units or aircraft APUs.

## THE TECHNICAL CHALLENGES OF MCR

The foregoing advantages of MCR and its compatibility with ongoing initiatives for future gas turbine engines make the concept worthy of further study especially to specific areas in which the inherent benefits could be best applied. However, serious development of MCR presents many challenges.

Thermal Management

The MCR concept as applied to the hot end (the most difficult) of a gas turbine engine would require formidable thermal management; a superconductor operating at 50°K adjacent to an HP Turbine operating at 1700°K defines the challenge. Figure 4 shows a method of addressing the requirement.

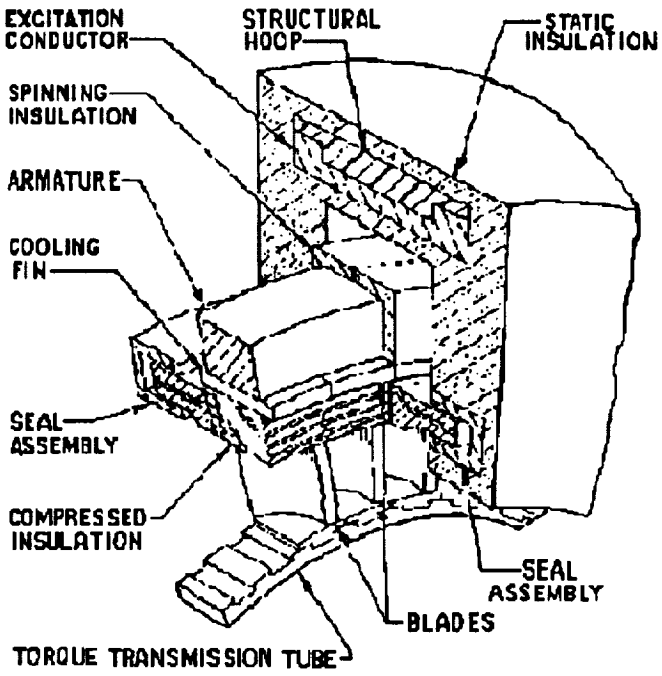


Figure 4: Schematic of Possible MCR Design

Compressed insulation would limit the amount of engine heat reaching the superconductor and would also need to transmit the centrifugal loads evenly to the cooling fin and armature. The material selected would need to be strong, (20 ksi compressive strength) lightweight, of small volume and with an extremely low thermal conductivity (0.5 W/mK). Clearly, these are conflicting properties. From a variety of potentially suitable materials studied, Zirconia Y-TZP, with a compressive strength of 1750 MPa and a thermal conductivity of 2.7 W/mK, was found to have the best combination of properties. It might be that increasing the porosity of Zirconia would reduce further the thermal conductivity without significant detriment to the compressive strength

The cooling fin helps to dissipate the heat which passes through the compressed insulation. Cryogenic fluid would be delivered to the cooling fin edges and the fluid then passes out from small holes to the spinning insulation. The spinning insulation protects the armature from heat generated by rotational drag. Coolant from the cooling fin passes between the armature and the spinning insulation, exiting at the rotor tip and removing heat passing through the spinning insulation. This is shown in Figure 5. The final insulation surrounds the excitation conductor, structural hoop and coolant seals. This insulation would protect the MCR system from environmental heat sources and heat generated by rotational drag.

Lastly, coolant seals would provide two functions. Engine gases would be prevented from entering the area between the armature and excitation conductors thus helping to keep coolant requirement to a minimum. The seals would also help to limit the amount of coolant leaked into the engine gas stream; again, excessive leakage would increase the coolant requirement and, ideally, seal leakage rates should be less than rotor coolant requirements. The seals would need to withstand rotor tip speeds of 2000 ft/sec, which are much greater speeds than currently fielded seals operate at, and would need to operate at close clearances (< 0.001 in) yet be efficient over a comparatively large range. Compliant foil seal technology shows the potential for meeting these high demands.

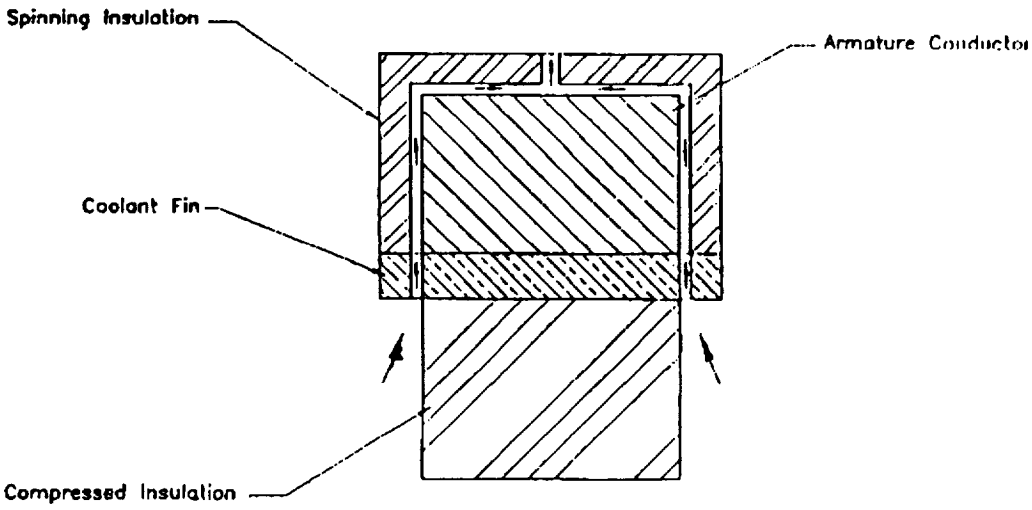


Figure 5: Flowpath of Coolant within Spinning Insulation

Other Potential Operating Difficulties.

The concept of a gas turbine engine operating without disks nor bearings is difficult to imagine. How does the rotating assembly sit when stationary; how does it spool up; and how does it remain axially stable when rotating? Similarly, what power does it consume in steady state; what happens in the event of power failure; and is there not a massive magnetic effect both for easy detection and to interfere with other systems in the aircraft? Finally, how is the superconductor temperature maintained at 50-100 K. These types of questions have been examined and most of them satisfactorily answered.

Electrical current is introduced into the outer (excitation) coil and the resulting opposing current in the inner (armature) coil is induced. During operation, changes in engine rotational speed would be accompanied by

Electrical current is introduced into the outer (excitation) coil and the resulting opposing current in the inner (armature) coil is induced. During operation, changes in engine rotational speed would be accompanied by an input or withdrawal of electrical power from the excitation coil so as to keep the magnetic pressure equal and opposite to the centrifugal force. The source of power for inputs to the excitation coil would be met from the MEA power capabilities; the electrical equivalent of an accumulator would meet this requirement. Similarly, withdrawal of power would be dissipated in some form of capacitor system. For initial start-up, the initial power into the excitation coil (100-300 kW for 4-5 secs) would lift and centralize the stationary rotor (armature) and then more power (probably as much again) would be introduced progressively as the rotational speed built up to ground idle rpm. This sequence would avoid crushing the rotor when it is not generating centrifugal force but a bigger concern is the structural integrity of the outer coil which ultimately has to withstand the centrifugal force. Superconductors currently tolerate around 0.5% strain which would, in the case of an MCR application with a 10 in radius, be 1/20 in increase. A strong, rigid structure in which to encase the outer coil would therefore be essential.

An envisioned large magnetic signature does not in practice occur. The flux density (T) decreases rapidly with distance both radially and axially from the armature as shown in Figure 6. Outside the MCR system, magnetic flux is less than that of stray fields from standard electric motors and appliances (0.05T). At a radial distance of less than 15 ft, the level is less than the world's background level (0.0001T). Therefore, neither detection by outside sources nor interference with engine controls is considered to be a problem.

Cooling of the superconductor is a more complex issue. Calculations based on the F110 engine suggest that approximately 50 kgs of liquid Hydrogen would be needed per hour to maintain the temperature. Hydrogen was chosen for the study because of its high cooling ability and its additional use as a fuel in the gas stream after it has cooled the superconductor. Clearly, the carriage of coolant for aircraft is a additional complexity and weight penalty and it might be that, in practice, a more efficient cooling method is used. Alternative methods include using fuel to first remove the "easy" heat followed by a cryocooler to remove the remaining "more difficult" heat.

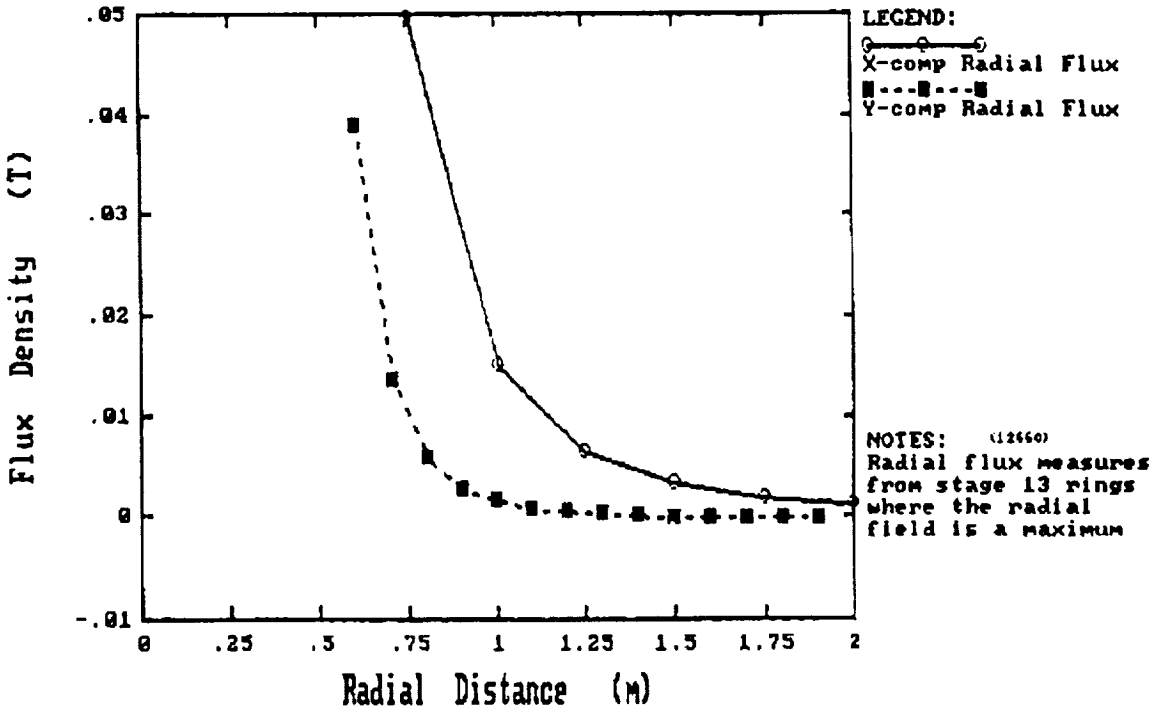


Figure 6: Magnetic Fields would be Low Outside a Gas Turbine Engine

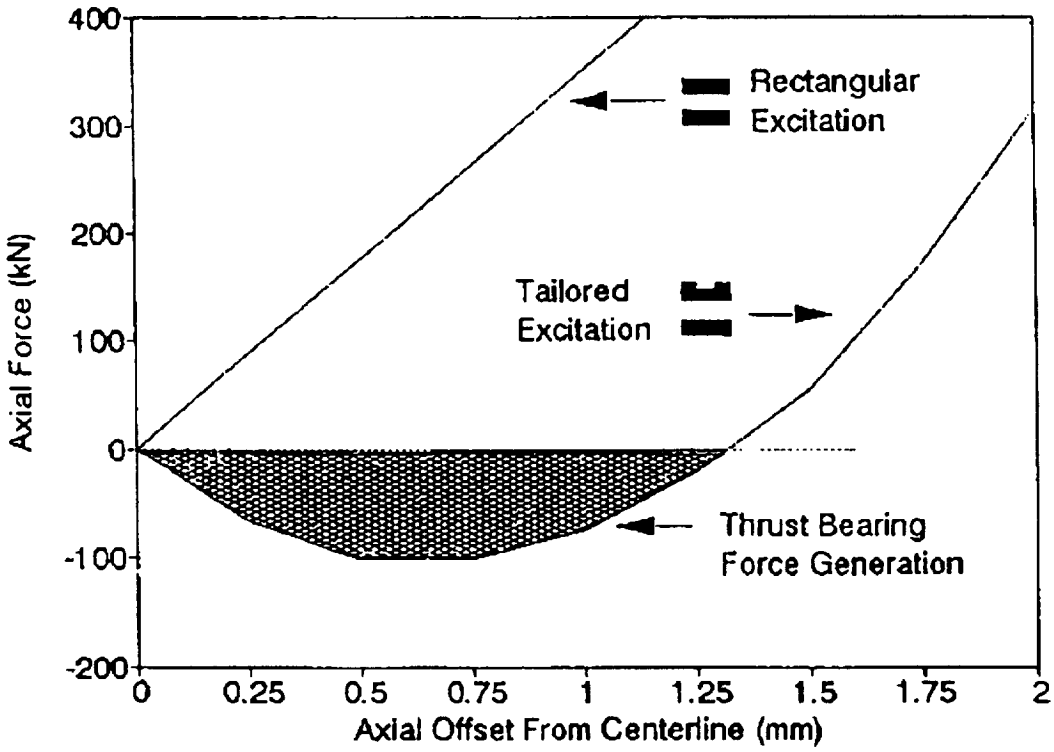


Figure 7: Shaping the Excitation Coil Creates a Magnetic Thrust Bearing

Stability is provided by the shapes of the excitation and armature conductors. Together the two conductors form a magnetic bearing. Radial stability occurs naturally as the MCR system is a radially stable magnetic bearing. Axial stability does not occur so readily but it can be achieved by concentrating excitation current on the outer edges of the excitation conductor. Figure 7 shows how shaping the excitation coil provides a specific magnetic thrust bearing capability.

## TECHNOLOGY TRANSFER POTENTIAL OF MCR

While the MCR concept has been proven in laboratory tests and its merits applied theoretically to aircraft gas turbine engines, the way forward is not so clear. What is clear, however, is the relevance of the concept to other applications. For the airborne application the benefits of weight savings and system simplicity which are believed to be possible need to be assessed in more detail and quantified. An engine study, whereby an existing engine was redesigned using MCR, would be a next logical step. Additionally, the build of a mock up single stage turbine based on the schematics seen earlier would provide greater insight into the real-life workings of the concept. These initiatives could take place in parallel with other R&D efforts to improve the capabilities of compliant foil seals, superconductors, and high-strength insulation materials such as Zirconia.

The potential of MCR lends itself to a variety of commercial applications. One obvious example is civil air transport especially if the weight-saving benefits and reductions in life cycle costs were fulfilled. Similarly, industrial gas turbines could benefit significantly from the possible reductions in system size and complexity and the likely increases in operating life of the rotating components. Finally, but not so obviously, MCR could be considered as a potential replacement for conventional bearings in almost all applications. This paper has taken the first step by spreading the awareness of an innovative concept whose potential is far-reaching and wide ranging; those who will potentially benefit from the concept need to take it further.

# *Full Wave Analysis of Passive Microwave Monolithic Integrated Circuit Devices Using a Generalized Finite Difference Time Domain (GFDTD) Algorithm.*

**Faiza S. Lansing**
California Institute of Technology
Jet Propulsion Laboratory
Pasadena, California

**Daniel L. Rascoe**
California Institute of Technology
Jet Propulsion Laboratory
Pasadena, California

## ABSTRACT

This paper presents a modified Finite-Difference Time-Domain (FDTD) technique using a generalized conformed orthogonal grid. The use of the Conformed Orthogonal Grid, Finite Difference Time Domain (GFDTD) enables the designer to match all the circuit dimensions, hence eliminating a major source of error in the analysis. The method proves to be a powerful and efficient tool for modeling complicated microstrip circuits. From the time domain results, the frequency-dependent parameters of a millimeter-wave branch line coupler, a dual-stub filter, and a 3-dimensional package are computed. Accuracy verification of the model is further achieved by comparing the results with those obtained from measurements, when available, and other commercial software tools.

## INTRODUCTION

Developing low-cost, compact, densely packed, and high-performance Monolithic Microwave Integrated Circuits (MMIC's) is a major technology thrust. To reduce the time and cost of the hardware iterative design cycle, and to increase the probability of first pass designs, rigorous analysis tools are needed to provide reliable predictions of the performance parameters.

Simple discontinuities, such as bends, tee- and cross-junctions, step in widths, etc., are basic components of any complex microstrip circuits [1 - 4]. To model such circuits, designers usually use the quasi-static analysis that is based on empirical low-frequency formulae. However, this quasi-static analysis does not accurately evaluate the characteristics of monolithic circuits at microwave or millimeter-wave frequencies since it does not account for radiation, coupling, fringing, and wave propagation effects. Some circuits, such as patch antennas, radial stubs, or spur filters, cannot be investigated using the quasi-static analysis because of the high radiation, and coupling effects. In such a case, more rigorous techniques, that provide an exact, or full-wave, solutions of Maxwell's equations are needed. One of the analysis tools, that is straight forward, versatile, and has acquired many new applications, is the Finite-Difference Time-Domain (FDTD), however the FDTD does not allow the designer to match all circuit dimensions. A new generalized 3-D conformed orthogonal grid, Finite Difference Time Domain (GFDTD) technique, presented in this paper, matches all circuit dimensions, and compensates for the deficiency in the FDTD technique. The GFDTD is designed to handle predominantly planar multilayered microstrip structures. Interlayer transitions such as striplines and vias can be easily simulated. The GFDTD proves to be flexible in handling a variety of complex circuit configurations.

Three sample structure are selected from a variety of test cases to demonstrate the versatility of the GFDTD technique and for the verification of the model. Three structures are modeled. A millimeter-wave branch line coupler fabricated on gallium arsenide (GaAs) substrate with $\varepsilon = 12.9$; a dual-stub low-pass filter fabricated on an Alumina substrate with $\varepsilon=9.9$, and a 3-Dimensional package fabricated on a Alumina substrate with $\varepsilon=9.9$. All the circuits represent resonant microstrip structures fabricated on an open substrate; hence, radiation and coupling effects dominate the performance significantly. The results of using the conformed orthogonal grid technique to the analysis of frequency-dependent scattering parameters and the performance of complex geometry printed microstrip circuits are presented. The GFDTD scattering parameters are further compared with the available measurements and computed results from a commercial software (nodal simulator) for the fabricated circuits.

## GOVERNING EQUATIONS

The GFDTD method begins by considering the partial differential form of the two Maxwell's curl equations that govern the propagation of electric and magnetic fields in structures.

$$\mu \frac{\partial \vec{H}}{\partial t} = -\nabla \times \vec{E} \tag{1}$$

$$\varepsilon \frac{\partial \vec{E}}{\partial t} = \nabla \times \vec{H} - \sigma \vec{E} \tag{2}$$

Where $\mu$ is permeability of the medium in henry/meter, $\varepsilon$ is the permittivity of the medium in farad/meter, $\sigma$ is conductivity of the medium in siemens/meter, E is electric field intensity in volt/meter, H is the magnetic field intensity in ampere/meter, and t is the time elapsed in seconds. To find an approximate solution to equations (1) and (2), the finite difference method is commonly used to discretize the three dimensional space and time domains and add the appropriate boundary conditions.

A. Finite-Difference Equations

In 1966, Yee [1] has developed a technique to solve the two Maxwell's curl equations. The six field components ($E_x$, $E_y$, $E_z$, $H_x$, $H_y$, $H_z$) are considered to be interleaved in space and are placed as shown in the elemental cell of Figure 1. The entire space domain no matter how complex it can be, is obtained by stacking these parallelepiped cells into a larger 3-D configuration. The x, y, and z dimension of the elemental cell are $\Delta x$, $\Delta y$, and $\Delta z$, respectively.

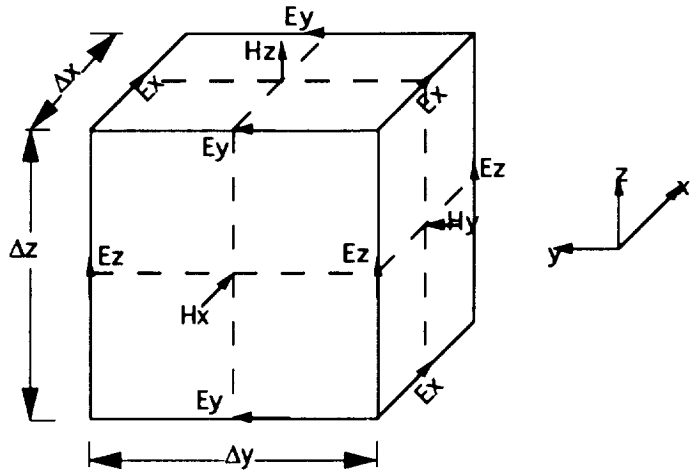


Figure 1. Field components placed in an FDTD elemental Cell (uniform grid)

Using the above arrangement notation for the E and H fields, the explicit finite difference forms of equations (1) and (2) for $E(\vec{r},t)$ and $H(\vec{r},t)$ are found [3].

B. Model Adaptation for Conformed Grids

The use of uniform grids, in most cases, contribute to errors [2]. To avoid such errors we adapted Yee's finite difference equations to suit conformed grids, producing the GFDTD technique, which offer a superior solution by avoiding errors resulting in mismatching the actual boundaries of the structure. As shown in Figure 2, electric field components (E white dots with black arrows, H in black dots) take new values at the boundaries between two consecutive non uniform spacing.

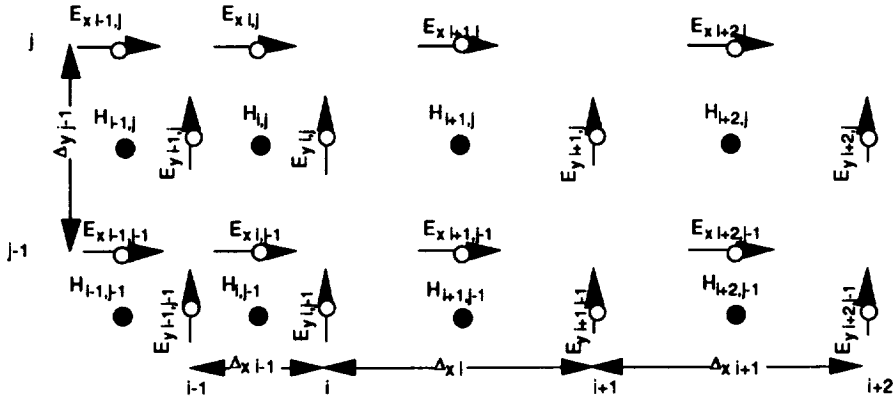

Figure 2. Field components in the x-y plane for a conformed grid

Hence, for conformed grids the finite difference equations for $H_X$, $H_Y$, $H_Z$ remain unchanged while equations are:

$$H_{xi,j,k}^{n+\frac{1}{2}} = H_{xi,j,k}^{n-\frac{1}{2}} + \frac{\Delta t}{\mu \Delta z}\left(E_{yi,j,k}^{n} - E_{yi,j,k-1}^{n}\right) - \frac{\Delta t}{\mu \Delta y}\left(E_{zi,j,k}^{n} - E_{zi,j-1,k}^{n}\right) \tag{3}$$

$$H_{yi,j,k}^{n+\frac{1}{2}} = H_{yi,j,k}^{n-\frac{1}{2}} + \frac{\Delta t}{\mu \Delta x}\left(E_{zi,j,k}^{n} - E_{zi-1,j,k}^{n}\right) - \frac{\Delta t}{\mu \Delta z}\left(E_{xi,j,k}^{n} - E_{xi,j,k-1}^{n}\right) \tag{4}$$

$$H_{zi,j,k}^{n+\frac{1}{2}} = H_{zi,j,k}^{n-\frac{1}{2}} + \frac{\Delta t}{\mu \Delta y}\left(E_{xi,j,k}^{n} - E_{xi,j-1,k}^{n}\right) - \frac{\Delta t}{\mu \Delta x}\left(E_{yi,j,k}^{n} - E_{yi-1,j,k}^{n}\right) \tag{5}$$

$$E_{xi,j,k}^{n+1} = \left[\frac{1-\frac{\sigma \Delta t}{2\varepsilon}}{1+\frac{\sigma \Delta t}{2\varepsilon}}\right] E_{xi,j,k}^{n} + \frac{1}{1+\frac{\sigma \Delta t}{2\varepsilon}}\left\{\frac{2\Delta t}{\varepsilon\left(\Delta y_{j+1} + \Delta y_j\right)}\left[H_{xi,j+1,k}^{n+\frac{1}{2}} - H_{xi,j,k}^{n+\frac{1}{2}}\right] - \frac{2\Delta t}{\varepsilon\left(\Delta z_{k+1} + \Delta z_k\right)}\left[H_{yi,j,k+1}^{n+\frac{1}{2}} - H_{yi,j,k}^{n+\frac{1}{2}}\right]\right\} \tag{6}$$

$$E_{yi,j,k}^{n+1} = \left[\frac{1-\frac{\sigma \Delta t}{2\varepsilon}}{1+\frac{\sigma \Delta t}{2\varepsilon}}\right] E_{yi,j,k}^{n} + \frac{1}{1+\frac{\sigma \Delta t}{2\varepsilon}}\left\{\frac{2\Delta t}{\varepsilon\left(\Delta z_{k+1} + \Delta z_k\right)}\left[H_{xi,j+1,k}^{n+\frac{1}{2}} - H_{xi,j,k}^{n+\frac{1}{2}}\right] - \frac{2\Delta t}{\varepsilon\left(\Delta x_{i+1} + \Delta x_i\right)}\left[H_{zi+1,j,k}^{n+\frac{1}{2}} - H_{zi,j,k}^{n+\frac{1}{2}}\right]\right\} \tag{7}$$

$$E_{zi,j,k}^{n+1} = \left[\frac{1-\frac{\sigma \Delta t}{2\varepsilon}}{1+\frac{\sigma \Delta t}{2\varepsilon}}\right] E_{zi,j,k}^{n} + \frac{1}{1+\frac{\sigma \Delta t}{2\varepsilon}}\left\{\frac{2\Delta t}{\varepsilon\left(\Delta x_{i+1} + \Delta x_i\right)}\left[H_{yi+1,j,k}^{n+\frac{1}{2}} - H_{yi,j,k}^{n+\frac{1}{2}}\right] - \frac{2\Delta t}{\varepsilon\left(\Delta y_{j+1} + \Delta y_j\right)}\left[H_{xi,j+1,k}^{n+\frac{1}{2}} - H_{xi,j,k}^{n+\frac{1}{2}}\right]\right\} \tag{8}$$

The GFDTD forward difference approximation is used to calculate the spatial partial derivatives instead of the centered difference used in equations [1-4]. The forward difference technique is first-order accurate, which may cause slight errors, when integrating for a large number of time steps. With this fact in mind, the GFDTD is only applied to determine the E fields at the boundaries of two consecutive layers of different spatial size, while Yee's equations [1] are used to compute the E fields within each layer. Also, the reader should be aware that the changes in spatial increment between layers is restricted to $\pm 30\%$. Better accuracy can be achieved if an interpolation technique is used, such as a spline to determine the spatial partial derivative of the magnetic field exactly at the interface between the two different layers.

C. Selection of size of Time Step

For the conformed grid, the size of the time step is based on modifying the stability criteria [2] to take into consideration the changing spatial steps. For $l$ number of $\Delta x$'s, $m$ number of $\Delta y$'s, and $n$ number of $\Delta z$'s, the size of time step in a conformed grid computation, is determined from:

$$\Delta t \le \min\left[\frac{1}{v_{max}}\left(\frac{1}{\Delta x_i^2}+\frac{1}{\Delta y_j^2}+\frac{1}{\Delta z_k^2}\right)^{-\frac{1}{2}}\right] \tag{9}$$

Where i=1, 2,... $l$; j=1,2,... $m$; k=1,2, ..$n$ and $\Delta t$ is chosen as the minimum of the permutation generated by varying i, j, k.

Equations (3) through (9) give an approximate solution of $E(\vec{r}, t)$ and $H(\vec{r}, t)$ in the computational domain (or grid). Special considerations are required, however, for the source and the mesh walls, as discussed in section D.

D. Treatment of the Source, and Absorbing Boundary Conditions

1. Source Considerations

A Gaussian-shaped pulse is chosen as the source excitation at time t=0. This choice is advantageous because its frequency spectrum is also Gaussian. By adjusting the width of the pulse, the spectrum provides frequency-domain information ranging from dc to the desired cutoff frequency .

$$E_z = f_s(t) = e^{-\frac{(t-t_o)^2}{T^2}} \tag{10}$$

The Gaussian-shaped pulse excitation will result in the fundamental mode propagating down the microstrip in the frequency range of interest.

2. Absorbing Boundary Conditions

One of the six mesh boundaries is a ground plane and its tangential electric field values are set to be zero everywhere on the plane. The tangential electric field components on the remaining five mesh boundaries must be specified such that outgoing waves are not reflected, i.e., absorbed. Mur's [5] second-order approximate absorbing boundary condition is used to enforce the above non-reflection constraints, as shown below:

$$\begin{aligned}\Phi_0^{n+1} = &-\Phi_1^{n-1}(i,k) + \frac{c\Delta t-\Delta y}{c\Delta t+\Delta y} + \frac{2\Delta y}{c\Delta t+\Delta y}\left[\Phi_0^n(i,k)+\Phi_1^n(i,k)\right] \\ &+ \frac{(c\Delta t)^2\Delta y}{2\Delta x^2(c\Delta t+\Delta y)}\left[\Phi_0^n(i+1,k)-\Phi_0^n(i,k)+\Phi_0^n(i-1,k)+\Phi_1^n(i+1,k)-\Phi_1^n(i,k)+\Phi_1^n(i-1,k)\right] \\ &+ \frac{(c\Delta t)^2\Delta y}{2\Delta z^2(c\Delta t+\Delta y)}\left[\Phi_0^n(i,k+1)-\Phi_0^n(i,k)+\Phi_0^n(i,k-1)+\Phi_1^n(i,k+1)-\Phi_1^n(i,k)+\Phi_1^n(i,k-1)\right]\end{aligned} \tag{11}$$

Where c is the speed of light in vacuum, $\Phi$ is the desired parameter to absorbed at the boundaries. Note that this expression is valid only for the x-z plane. Similar expressions can be derived for x-y and y-z planes

E. Calculation of Frequency-Dependent Parameters

In addition to the time domain results (E, H, voltages, and currents), obtained by the GFDTD method, the frequency-dependent scattering parameters, characteristic impedance, and effective dielectric constant, which augment the analysis are calculated.

The scattering parameters provide a measure for the circuit performance. To calculate scattering parameters, the total vertical electric field underneath the center of each microstrip port is recorded at every time step and integrated along the z-direction as shown in figure 3-a. To obtain the scattering parameter $S_{11}(\omega)$, the incident and reflected voltage must be determined by calculating the incident and reflected voltages at the input port (port 1). The incident voltage, $V_{1inc}$ is determined by assuming an infinite microstrip line, which extends from

source to the far absorbing wall,. The same process is repeated using the actual microstrip structure, yielding the total voltage, $V_{1t}$ at the input port. The reflected voltage, $V_{1ref}$ is determined by subtracting the incident voltage from the total voltage at the input port. At the other ports only transient waveforms will be computed. The scattering parameters, $S_{11}$, $S_{21}$, and $S_{12}$ are then obtained by simple Fourier transform of the voltages. The current I(t) is computed at the port by integrating the magnetic field over the contour C as shown in Figure 3-b.

The characteristic impedance, $Z_0(\omega)$ of a microstrip line is defined at the fundamental mode of propagation, as the ratio of the voltage to the current in the frequency domain.

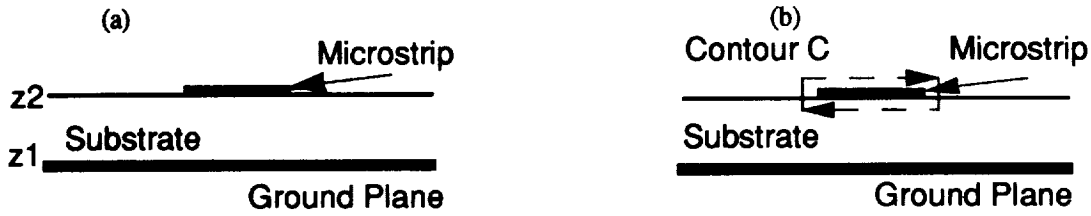


Figure 3 Configuration for computing the total voltage and current at the ports

## RESULTS

The three structures used in testing the GFDTD model with conformed grid are as follows: a branch line coupler; a dual stub filter; and a 3-dimensional package. The first circuit is fabricated on gallium arsenide (GaAs) substrate with $\varepsilon$= 12.9 and a thickness of 100 $\mu$m. The dual stub filter is constructed on Alumina substrate with $\varepsilon$=9.9 and a thickness of 0.005 inch (0.127 mm), and a 3-dimensional package fabricated on an Alumina substrate with $\varepsilon$= 9.9 and a thickness of 0.3 millimeters. The three circuits have dimensions of less than 1 cm, and the frequency range of interest is from dc to 50 GHz. Although the operating frequency of all circuits is less than 50 GHz; the GFDTD is able to provide an insight to the performance of these circuits outside the operating range. Scattering matrix coefficients are measured for the dual stub filter, the using an HP 8510 network analyzer, which is calibrated between 2 to 45 GHz. Measurements for the millimeter-wave branch line coupler and the 3-D package are not available.

### A. Millimeter-wave Branch Line Coupler

The selected branch line coupler, is shown in Figure 4, divides power equally between ports 2 and 4 from either ports 1 or 3. This occurs at the center frequency, where the center-to-center distance between the four lines is a quarter wavelength ($\lambda$/4). Also, at the center frequency, the phase difference between ports 2 and 4 is 90°. The total number of grid points is 49x100x 16. The thickness of the substrate is modeled as 3 $\Delta$z, while the air space above is modeled as 13 $\Delta$z.

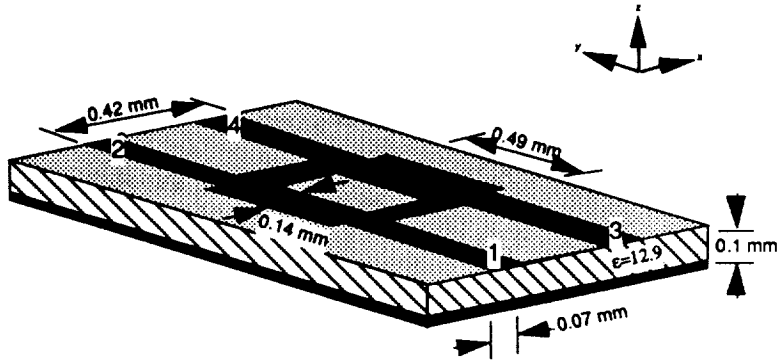


Figure 4. Millimeter-wave branch line coupler detail.

The center to center distance are 14 $\Delta$x and 14 $\Delta$y. The distance form the source plane to the edge of the coupler is 40 $\Delta$y, and the reference planes for ports 1 through 4 are 10$\Delta$y from the edges of the coupler. The strip widths of ports 1 through 4 are modeled as 2 $\Delta$x. The wide strips in the coupler are modeled as 4 $\Delta$x wide.

The time step $\Delta t$ is 0.05 ps. The Gaussian half-width, T is 5 ps and the time delay, $t_0$, is set to 3T. The simulation is performed for 4000 time steps to allow the response on all four ports to reach zero. The computation time using the CRAY Y-MP2E/116 is less than 2 minutes for the conformed grid.

The scattering coefficient results, are shown in Figure 5. The desired branch line coupler performance is witnessed in the sharp $S_{11}$ and $S_{13}$ nulls which occur at approximately the same point (49 GHz) as the crossover in $S_{12}$, and $S_{14}$. At this crossover point $S_{12}$ and $S_{14}$ are both about -3 dB, indicating that the power is being evenly divided between ports 2 and 4. The nulls in $S_{11}$ and $S_{13}$ at the operating frequency indicate that little power is being transmitted by ports 2 and 4. The phase difference between $S_{12}$ and $S_{14}$, is verified to be approximately 90° at the operating point (≈49 GHz). This behavior is also predicted by Compact Explorer software.

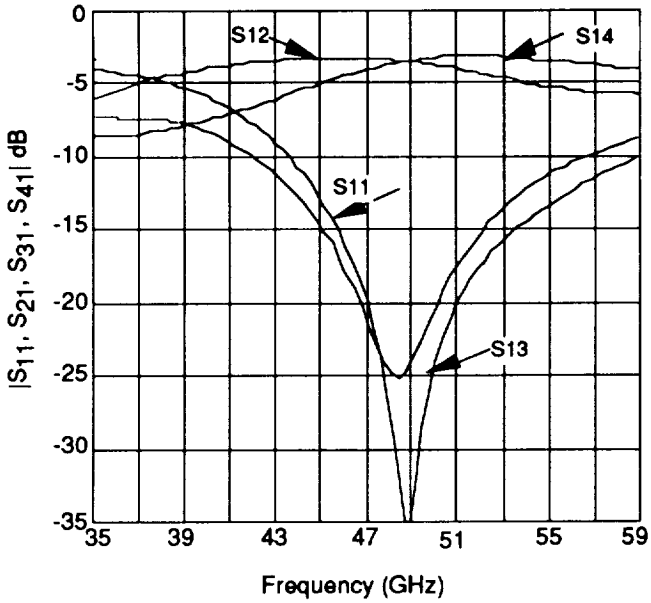


Figure 5 Scattering parameters for the millimeter-wave branch line coupler

B. Microstrip Dual-Stub filter

The dual stub filter analyzed is based on the design used by Texas Instrument and the University of Colorado, MIMICAD Center [6]. The dimensions are shown in Figure 6. The total number of grid points representing this filter is 120x68x16. The operating resonance ( ≈ 10 GHz) corresponds to the frequency where $L=\lambda/4$, and $S=\lambda/16$and the distance between the center of each stub and the ports is $\lambda/32$ For the GFDTD, 2 $\Delta x$, 2 $\Delta y$, and one $\Delta z$ are carefully chosen to fit the dimensions of the circuit. The long rectangular patch is thus $2\Delta x$'s by $68\Delta y$'s. Each stub is modeled as $46\Delta x$ by $2\Delta y$. The thickness of the substrate is selected as 2 $\Delta z$, the remaining 14 $\Delta z$ represent the air space above the substrate.

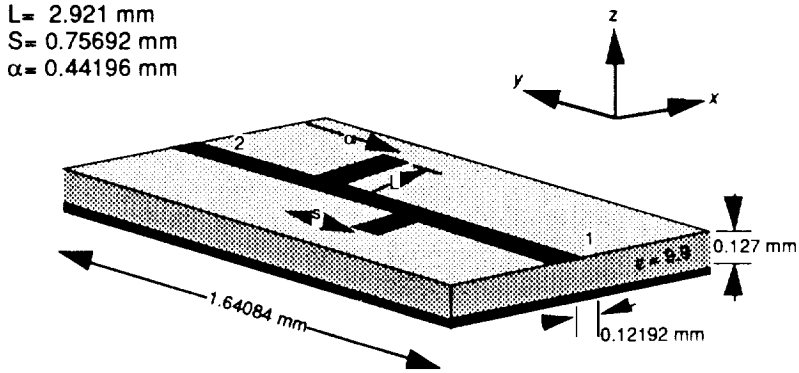


Figure 6 Double-stub filter detail

The time step, $\Delta t$ used is 0.117 ps. The Gaussian half-width is T= 10 ps and the time delay $t_0$ is set to be 3T. The simulation is performed for 15000 time steps to allow the response at both ports to become 0. Due to the circuit higher dielectric constant, the phase speed is lower and more samples, i.e., time steps, are needed to fully simulate the behavior of the circuit. The computation time for this circuit is approximately 18 minutes on the CRAY Y-MP2E/116 compared to 2 hours per each frequency for an HP workstation [6].

The resulting scattering coefficient $|S_{21}|$ is plotted in Figure 7-a for GFDTD, superimposed on the measured data. Good agreement is evident at the location of the response nulls. The desired low-pass filter performance is witnessed by the steep $S_{21}$ roll-off beginning at approximately 8 GHz. The narrowing in the stopband determined from the GFDTD model, may be due to the approximation of using the forward difference technique for the conformed grid. In comparing the scattering parameters determined from measurements with the results determined from the nodal simulator, shown in figure 7-b it is obvious that the nodal simulator, lacks the capability to predict the performance of this filter. Additionally the nodal simulator is unable to predict the dual response nulls as expected from having dual stubs but is predicts correctly the location of one resonating frequency qualitatively and overestimates the depth of the response nulls.

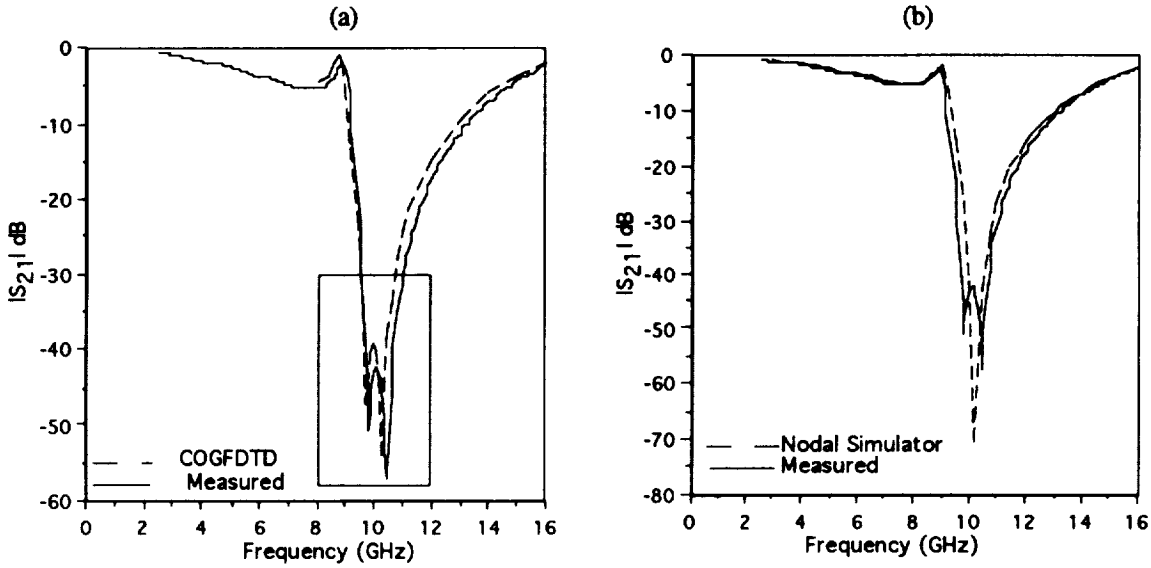


Figure 7 Insertion loss of a dual stub filter

C. 3-Dimensional Package

The 3-Dimensional Package is designed and fabricated on an Alumina substrate with $\varepsilon$= 9.9. The 3-D package dimensions are shown in Figure 8. The space steps $\Delta x$ ,$\Delta y$, and $\Delta z$ are chosen to match all circuit dimensions. This circuit is the most complicated, in all the cases treated in this paper, because it has multilayers. The total physical dimension of this package is 9 mm x 4.02 mm x 3 mm, which transferred 67x150x61 grid points. The thickness of the substrate is modeled as 10 $\Delta z$ while the air spaces above and below the substrate are modeled as 25 $\Delta z$ each.

The design procedure presented in [7] have been followed carefully for this circuit to yield the desired performance parameters.

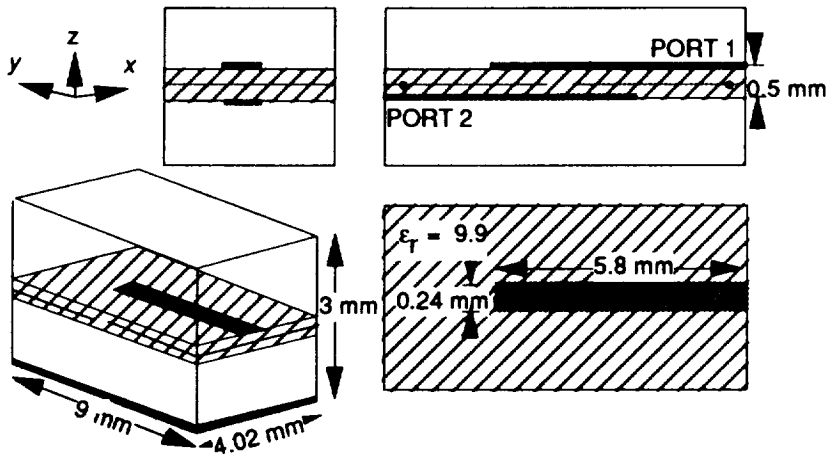


Figure 8. Detail of 3-Dimensional Package

The time step $\Delta t$ is 0.1 ps. The Gaussian half-width, T is 15 ps and the time delay, $t_0$, is set to 3T. The simulation is performed for the GFDTD for 3000 time steps to allow the response on the two ports to reach zero. The computation time using the CRAY Y-MP2E/116, is less than 10 CPU minutes

The frequency response presented in figure 9, demonstrates the utility of this structure as an interconnect. The desired frequency response, i.e., center frequency, bandwidth, and shape is obtained by the proper selection of geometry. As shown in figure 9, the insertion loss at the center frequency is less than 0.2 dB and a very wide bandwidth is achievable, which makes this design versatile specially at higher frequencies.

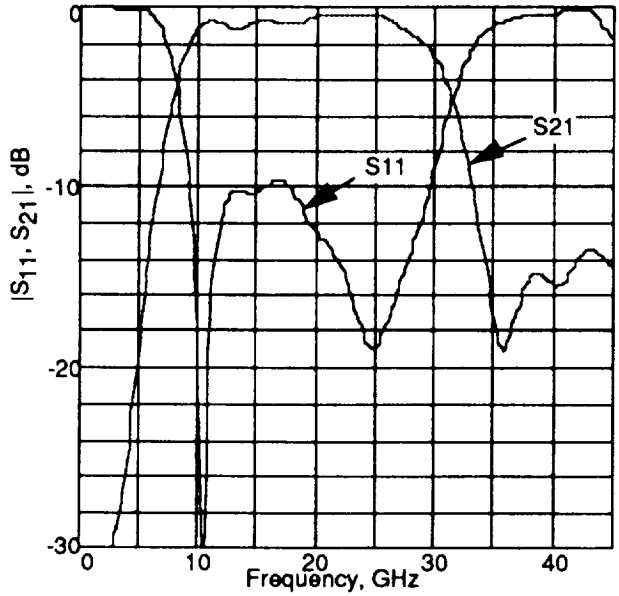


Figure 9. Scattering parameters for the 3-Dimensional Package

## CONCLUSIONS

For the conformed orthogonal grid, the Generalized finite-difference time-domain method, GFDTD, has been used to perform time-domain simulations of pulse propagation in three printed microstrip circuits. Frequency-dependent scattering parameters, and characteristic impedance, have been calculated by Fourier transform of the time-domain results. The results are validated either by comparison with the results obtained from measured data taken from fabricated circuits, or results obtained from the nodal simulator. The versatility of the GFDTD method allows easy and accurate calculation of many complicated microstrip structures. It should be noted that simpler models, such as nodal simulator, are still highly useful for "first cut designs" of microstrip circuits since they allow

for quick solution and, in some cases, allow for intuition about devices being modeled. The GFDTD method can then be applied to determine the performance of the actual circuit more accurately.

The versatility of the GFDTD method allows for matching all circuit dimensions and for direct calculation of performance parameters for many complicated microstrip structures. The structures analyzed in this paper were selected so that comparisons could be made with other publications or measurements or methods of analysis. With the computational power of supercomputers increasing rapidly, such as the CRAY Y-MP2E/116, time savings in the order of 200 to 1 is achieved compared to the VAX workstation. The fast, accurate, GFDTD now lends itself as a computer aided design of many complex geometries of microstrip circuit components.

A video tape that visualizes the electric and magnetic fields as they evolve in time was produced.

## ACKNOWLEDGMENT

This research was carried out in part by the Jet Propulsion Laboratory, California Institute of Technology, under a grant with the National Aeronautics and Space Administration. This research was also performed in part using the Jet Propulsion Laboratory/California Institute of technology CRAY Y-MP2E/116 Supercomputer. Access to this facility was provided by the Jet propulsion Laboratory Supercomputing project.

## REFERENCES

[1] K. S. Yee, "Numerical solution of initial boundary value problems in isotropic media," *IEEE Transactions on Antennas and Propagation*, vol. AP-14, pp. 302-307, May 1966.

[2] D. Sheen, S. Ali, M. Abouzahra and J. A. Kong, "Application of the three-dimensional finite-difference time-domain method to the analysis of planar microstrip circuits," *IEEE Transactions on Microwave Theory and Techniques*, vol. 38, pp. 849-856, July 1990.

[3] X. Zhang, J. Fang, K. Mei and Y. Lui, "Calculations of the dispersive characteristics of microstrips by the time-domain finite difference method," *IEEE Transactions on Microwave Theory and Techniques*, vol. 36, pp. 263-267, July 1988.

[4] X. Zhang and K. Mei, "Time-domain finite difference approach to the calculation of the frequency-dependent characteristics of microstrip discontinuities," *IEEE Transactions on Microwave Theory and Techniques*, vol. 36, pp. 1775-1787, July 1988.

[5] D. M. Sheen, " Numerical Modeling of Microstrip Circuits and Antennas". Ph.D. dissertation, Massachusetts Institute of Technology, June 1991.

[6] Private communication with Dr. Doris Wu, MMICAD Center, University of Colorado, Boulder, Mars 1992.

[7] Vandenberg, N. L., "Full-Wave Analysis of Microstrip-Fed Antennas and Couplers", Ph.D. dissertation, The University of Michigan, 1991.